
The threedimensional view and distances of planetary nebulae

Hektor Monteiro¹ and Hugo E. Schwarz

Núcleo de Astrofísica Teórica - CETEC-UNICSUL, Rua Galvão Bueno, 868 São Paulo - SP CEP 01506-000, Brasil hektor.monteiro@gmail.com

Summary. Traditional 1-D empirical methods used to study Planetary Nebulae (PNe) gave distances to typically a factor of 3 or more with the associated very large uncertainties on the physical parameters of the objects. By taking a 3-D view of Planetary Nebulae (PNe) we show that the large uncertainties associated with classical methods of modeling and observing PNe to obtain their 3-D structures, distances and physical parameters are significantly reduced. Using long slit or Integral Field Unit spectrophotometry to constrain modern 3-D photoionization models for PNe, we determine detailed 3-D structures, central star parameters, and distances accurate to 10-20% by eliminating the uncertainties in the spatial structure determination and filling factor assumptions.

Key words: planetary nebulae, photoionization models, mapping, spectroscopy

1 Introduction

Planetary Nebulae (PNe) are the visible ionized results of the final evolutionary stage of most low- to intermediate mass stars, during which between 0.2 and more than $1 M_{\odot}$ is lost to form a low density envelope around the hot, dense stellar core of around $0.6 M_{\odot}$ which is left to contract at constant luminosity —but increasing it's temperature to the point that the matter surrounding the star is ionized and therefore made visible— and then to cool along evolutionary tracks in the left lower part of the HR diagram to eventually die as cold, invisible embers.

PNe have been used as Galactic low density plasma laboratories, to trace stellar populations in the Galaxy, and in and between other galaxies, and as standard candles to determine extragalactic distances. General discussions of all aspects of PNe research have been published by [8] and [4] and more recently in a review by [1].

One of the most important problems in observational Galactic PNe research is the difficulty in determining their distances and three-dimensional structures. Observations always produce a 2-D projection of their 3-D structure, and recovering the original structure is not trivial. This is also made worse by the fact that only crude distances, usually obtained from statistical methods on large samples, can

be determined. Large uncertainties are generated by the need to assume constancy of one parameter such as the nebular size, (ionized) mass, flux etc. so that typical errors in the distances to individual objects are of the order of a factor of 3 or more. Very few nebulae have had individual accurate distances determined.

2 The Method

Our work has tackled the problem of determining the structure and distances by applying 3-D photoionization models to PNe. The models are simultaneously constrained by fluxes in several emission lines, the angular size of the emission line maps in these lines, and the density maps of the nebula. By starting with a simplified 3-D structure for the nebula based on the appearance of the line and density maps and using an iterative procedure to refine the structure and fit to all lines simultaneously, we arrive at a model nebula that fits best the observed data. As inputs we also have a central star luminosity, temperature and chemistry of the gas, which are also varied until best fitting values are found. In this way the 3-D structure, ionizing source characteristics and chemistry of the gas as well as the distance are determined self-consistently and with much higher precision than has so far been possible. See [9] and works cited therein for more details on our method and 3-D photoionization codes. Below we describe the types of observations used to constrain our models and the photoionization code used.

2.1 Spatially Resolved Observations

Typically the observations used in the study of PNe are long-slit spectroscopy and narrow band imaging which usually suffice for the traditional empirical studies. However, to define a 3-D model we need comprehensive set of constraints to limit degenerate model solutions. For 3-D models the ideal set of constraints are spatially resolved, whether they are line images or diagnostic ratios. To achieve this we use two types of observations, spectro-photometric mapping and more recently integral field spectroscopy.

Spectro-photometric mapping is done by taking exposures at several parallel long-slit positions across the nebula. The line intensity profiles for each slit are then combined and interpolated to create emission line images of the nebula with a spatial resolution that is determined by the long-slit setup and number of slits observed, in a way similar to radio mapping (see Fig. 1). This procedure is quite useful since it allows for spatially resolved maps to be created for any line with significant signal. These maps can then be used to obtain the usual diagnostic ratios, now spatially resolved.

This technique also allows for interesting possibilities, for example, detecting scattered light from a Wolf-Rayet type star in its nebula, as we have done for NGC 40. In this case we were able to separate the wide component from a narrow component of the line CIII 4650. The wide component, which is produced only by the central star, is detected out to about 20 arcsec from the central source and thus can only be a result of scattering. Notice that traditional narrow-band imaging would not have been able to detect this. Further study is being carried out on this subject.

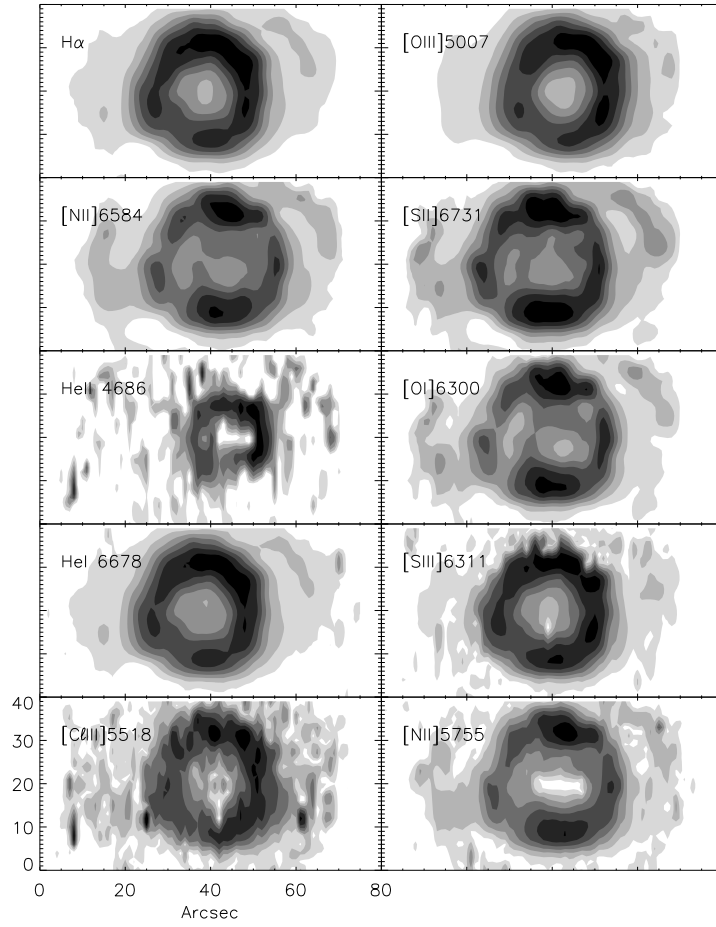


Fig. 1. Line maps generated from several long slit spectra taken across NGC 6369 taken from [6]. The maps have been corrected for reddening using the $H\alpha/H\beta$ extinction map.

2.2 Model Fitting

We use the Mocassin photoionization code described in detail in [3]. The input parameters are the elemental abundances, the gas density distribution, the shape and intensity of the central ionizing radiation spectrum (temperature, H and He absorption edges, and luminosity in the case of a star) and the distance to the object. The code then provides the physical conditions in each point of the nebula, i.e., ionic fractional abundances, electronic temperature and density, as well as the emission line luminosities of each cell.

This output is then used to produce projected images and total fluxes for a given number of emission lines and a set of (x,y,z) orientation angles. This output can then

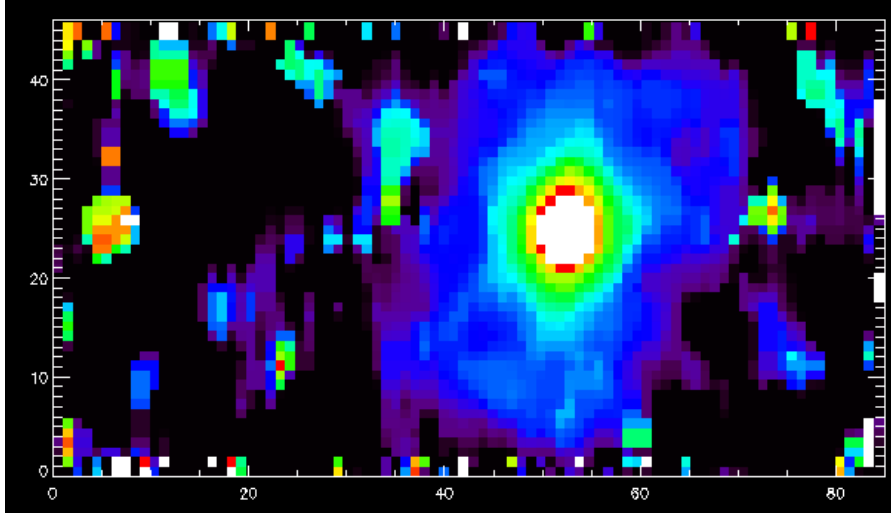


Fig. 2. Map of the scattered wide component of CIII 4650 produced by the Wolf-Rayet central source of NGC40.

be tailored to match given observational configurations such as single long slits, or multiple slits. From the projected images we can also construct projected diagnostic maps, such as density and temperature maps.

The model generated or simulated “observations” discussed above are then compared to the actual observational data obtained (in this case, the spectrophotometric mapping of Mz1 studied in [7]). We compare total line intensities and check for discrepancies. If one or more of the intensities are out of the range of the observational errors, we proceed to fine tune input parameters that have influence on the given line. For example, we take the $H\beta$ total fluxes from the model and observations and compare them. The $H\beta$ line is mainly dependent on the star luminosity and the 3-D structure of the gas, so we adjust these input parameters accordingly. In this case it is important to realize that the 3-D structure is actually defined by the density in each cell and a physical size for the object which is dependent on the distance. So in fact we are dealing with two input parameters when we consider the $H\beta$ flux. The same type of comparison is made for other lines such as [OIII]500.7nm which is an important coolant, HeII468.6nm which depends mainly on the CS temperature, among others. We also compare the model projected images and diagnostic maps to those obtained from the observations.

After fitting all the model constraints to their respective observational counterparts and adjusting the input parameters of the code accordingly, we calculate another model. The same procedure discussed above is then repeated until we reach a satisfactory agreement between model and observations for all line images, fluxes, diagnostic maps, etc.).

Notice that, after this iterative procedure, we obtain model fitted values for the input parameters that are self-consistently determined; they are the ionizing star characteristics, gas chemical abundances, density, structure, and distance.

One of the main differences of this procedure when compared to previous model calculations in the literature, is that we use the distance as a fitting parameter for the model. This is possible because we now have a way of producing projected images from the 3D model results and can therefore compare them directly with observed ones as well as the observed total fluxes. In other words, we do not use a fixed distance for our model calculations and vary only star and gas parameters (luminosity and temperature of the star, abundances and densities of the gas). The other important advantage of using the 3-D structure for the gas is the possibility of eliminating the need for a “filling factor”. This has major implications on the model parameters that can be determined, especially on the distance.

Since we use a 3-D structure that is consistent with observed images, position-velocity diagrams, diagnostic ratios (such as density maps) we are not making any assumptions about filling factors, ionized masses or physical sizes. All these parameters are determined self-consistently in the model.

The uniqueness of the solution obtained by this procedure can be argued of course. It is immediately clear that within the observational uncertainties there are an infinite number of solutions that can fit the observations. In other words, the observations determine the quality of the final parameters. In fact, if we estimate the goodness of fit of our model fit by quadratically summing all uncertainties and dividing by the number of observables minus the number of degrees of freedom (input parameters to the model), we get an error of about 20% in the case of Mz1. This is the uncertainty adopted for our results. The precise determination of fitting errors is extremely complex and given the nature of the 3-D code neither practical nor useful.

For the above reasons our distance determinations are fundamentally different from, and much more precise than classically found distances.

The mass of the ionizing source, as well as its progenitor and age are determined from theoretical cooling tracks. We have used the cooling tracks of [12] because their grids present a close sampling of progenitor masses in the 1 to $3M_{\odot}$ range.

3 Conclusions

The central star properties of all PNe that we have applied our method to are shown in the HR diagram of Fig. 3. Also shown are the values determined by other methods, taken from the literature. There are large differences between our values and those previously published for NGC 6781 and NGC 6369 and in both cases the central star luminosity determined by our method was higher than the literature value. This is because it was assumed that these nebulae are radiation bound but we have shown them to be matter bound as they lose up to 70% of their UV radiation to space, resulting in an underestimation of both the luminosity and temperature. The blue rise in the SED for NGC 6781 also confirms that blue radiation is escaping from the nebula. Note that the central star luminosity from our model, $L = 385/L_{\odot}$ is larger than the luminosity derived from the observed SED $L = 225/L_{\odot}$ by a factor of 1.7, confirming that the nebula is matter bound and that a significant fraction of the stellar UV flux escapes from the object. We believe our luminosities and temperatures are the more accurate ones that have been determined for these stars to date. Interestingly our values tend to bring the core masses closer to $0.6 M_{\odot}$ which is also close to the peak value of the narrow mass distribution of white dwarfs.

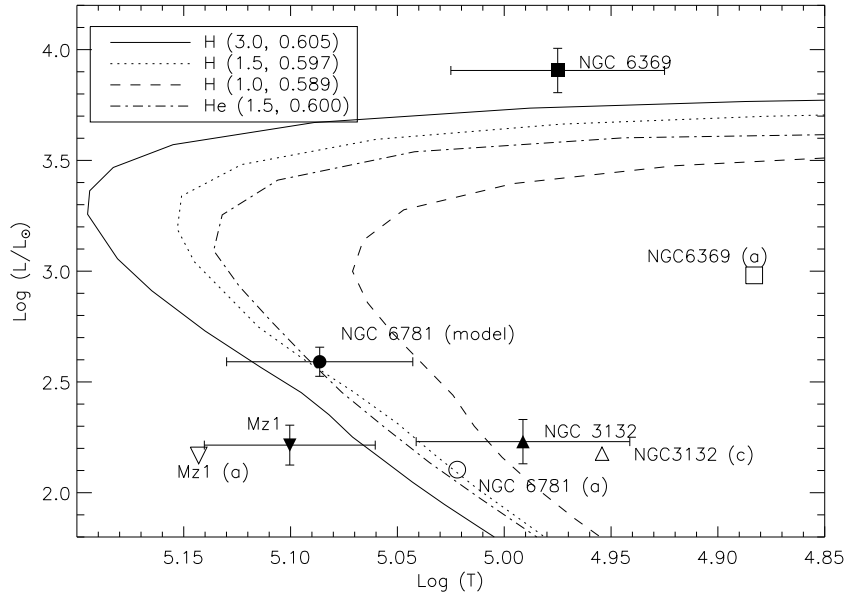


Fig. 3. HR diagram for NGC 6781, NGC 3132 ([5]), NGC 6369 ([6]), MZ 1 ([7]), all PNe that had their central star properties determined by our method. Also plotted are the literature values for comparison. a) [10]; b) [11]. The evolutionary tracks are from [12]; they are similar to the [2] models but take metallicities etc. into account.

References

1. Balick, B., & Frank, A. 2002, ARAA, 40, 439
2. Blöcker, T. 1995, A&A, 299, 755
3. Ercolano, B., Barlow, M. J., Storey, P. J., & Liu, X.-W. 2003, MNRAS, 340, 1136
4. Gurzadyan, G. A. 1997, The Physics and Dynamics of Planetary Nebulae, XVI, 513 pp. 179 figs. 93 tabs.. Springer-Verlag Berlin Heidelberg New York. Also Astronomy and Astrophysics Library
5. Monteiro, H., Morisset, C., Gruenwald, R., & Viegas, S. M. 2000, ApJ, 537, 853
6. Monteiro, H., Schwarz, H. E., Gruenwald, R., & Heathcote, S. 2004, ApJ, 609, 194
7. Monteiro, H., Schwarz, H.E., Gruenwald, R., Guenther, K., & Heathcote, S.R. 2005, ApJ, 620, 321
8. Pottasch, S. R. 1984, Astrophysics and Space Science Library, 107
9. Schwarz, H. E., & Monteiro, H. 2006, ApJ, 648, 430
10. Stanghellini, L., Corradi, R.L.M., Schwarz, H.E. 1993, A&A, 279, 521
11. Stanghellini, L., Villaver, E., Machado, A., & Guerrero, M. A. 2002, ApJ, 576, 285
12. Vassiliadis, E., Wood, P.R. 1994, ApJS, 92, 125